Alternative methods for detecting the degeneration of electric drive train components

CoFAT 2016

J. Adermann, P. Wacker, L. Horlbeck, M. Baumann, M. Lienkamp
Institute of Automotive Technology
Technical University of Munich
Garching, Germany
adermann@ftm.mw.tum.de

***Abstract*—This paper shows a new method of detecting the degeneration of the electrical drivetrain in modern electric vehicles due to ageing, overload or manufacturing errors of the components by fusing sensor data with vehicle history data. This information will be used for an accurate range prediction and a residual value estimation of the electric vehicle. Furthermore, malfunctions of the drive train components can be detected. The methods introduced will be implemented as an online solution and are shown on a test vehicle. The traction battery is the focus of this paper, while the components inverter and motor are outlined and are the subject of further research.**

Keywords—battery electric vehicle; electric drivetrain; efficiency; ageing; degeneration

I. INTRODUCTION

Both, politicians and manufacturers, see electric mobility as one of the greatest impositions the automotive industry has faced since the last century. In order to meet the CO_2 fleet limit, most manufacturers see vehicles with hybrid drive trains as a bridging solution on the way to battery electric vehicles (BEV). After the emergence of using defeat devices by a German car manufacturer, the enforcement of federal emission laws and their surveillance could be handled more severely in the future. This fact can be regarded as a benefit to the BEV technology. The customers, however, still treat electric mobility with skepticism. This is mainly due to constant high costs of the traction battery, the comparable low range and an uncertain residual value. This paper will target the degeneration (efficiency decrease), which correlates with a reduction in value on a component basis. As stated by the ADAC (General German Automobile Association) [1] the drop in value of a battery electric vehicle is higher compared to combustion engine vehicles. The knowledge of degeneration from a component point of view is seen as important information for the owner, the manufacturer and the property insurer. Components could be reused, recycled or sold on a second life market as an alternative to a trade on the used car market (Baumann [2], Bowler [3] and Neubauer [4]). It is conceivable that a component change of the electrical drivetrain is mandatory in order to improve the residual value of future BEVs.

Having detailed knowledge of the efficiency parameters of the drivetrain components of a BEV, however, is a great challenge. The state of the art is that the range prediction, which correlates with the actual efficiency, is only done on a state of charge (*SOC*) basis of the battery, without parameter and efficiency fading taken into account. From a research point of view, several methods of estimating battery and motor parameters were introduced in the last decade. High effort in computation and the risk of instability, however, prevent commercial use today. This is why a new method is introduced in this paper that gives a reliable online solution for calculating the state of health of the traction battery, the inverter and electric motor.

In this paper, first the test bed—an electrified Smart—with all its components is described in *Chapter II*. The test bed is used in order to monitor frequently arising driving patterns. The commuter's cycle monitoring is presented as a component independent method of data comparison in order to derive fading trends due to the degeneration or ageing of the drivetrain components, which is outlined in *Chapter III*.

Chapter IV gives a detailed overview of state of the art algorithms for observing the traction battery of BEVs. Furthermore, a new method for the state of health (*SOH*) calculation is introduced. The degeneration process of the inverter and the electric motor is discussed conceptually in *Chapter V*. It should be outlined that the presented methods of observing the components are developed for online use. Due to limited computing power and memory, the results are not comparable to scientific benchmarks. Reliability and feasibility in this case are in the foreground.

II. ELECTRIC VEHICLE TESTBED

As the test bed for implementing the methods in *Chapter III* and *Chapter V*, a Smart 451 was chosen (*Figure 1*). At the Institute of Automotive Technology the smart was reequipped with an electric drivetrain. The inverter and the electric motor were bought by prototype suppliers. With an installed capacity of 22 kWh, a range of 200 km is possible under nominal conditions (NEDC).

Figure 1: FORELMO test bed

A. Mechanical parameters of the testbed

The AKOE electric motor (induction motor—IM) of Schwarz Elektromotoren GmbH was chosen because of the low costs and size. The electric motor was installed directly to the gearbox, which is fixed to the third gear (5.697 gear ratio). The alternating current is provided by an inverter (Supplier: DMC—Digital Motor Control GmbH) consisting of several H-bridges with commercial Mosfets (IRFS4115PBF). The traction battery, consisting of 8 modules with 14S 18P interconnection was planned and assembled, using Panasonic NCR18650PF (NCA) cells. The inverter and the battery modules are cooled by a liquid cooling circle controlled by the Electronic Control Unit (ECU) and based on component temperatures. That way all components operating under specified temperature conditions is guaranteed.

B. ECU- and Sensornetwork

The Battery Management System (BMS) consists of several intelligent units and sensors (*Figure 2*). Each battery module is equipped with a dedicated hardware. These hardware units measure the cell voltages of each serial string and the module temperature at two thermal hot-spots using a PTC (positive temperature coefficient) element. This information is sent via CAN to the BMS-ECU and an observing unit on a 25 ms time base. An additional sensor measures the system current and redundantly the total voltage of the battery system. On the BMS-ECU a real-time framework is implemented in embedded C. Based on the module's information, the security of the battery pack is ensured by actively shutting down the drivetrain in the case of an error. The BMS-ECU is responsible for triggering and observing the main relays and evaluating the sensor information. The switch commands are derived automatically by the framework with respect to the driver request and battery operating conditions.

In addition to the BMS measuring modules and the BMS-ECU, an observer unit (OBS in *Figure 2*) is installed. The observer receives the CAN messages from the BMS measuring modules and the current sensor. The algorithm for the state estimations, which are introduced in *Chapter IV.B*, are generated with an automatic code generator from Simulink and are integrated into an embedded Linux system with additional driver components on the observer unit. Using this toolchain it is possible to implement and parametrize various algorithms with low programming effort and a short roundtrip time. Furthermore, a Model-in-the-Loop simulation can be directly compared to a Processor-in-the-Loop simulation in order to minimize implementation or scaling errors. Thereby, it can be verified that the simulation merits match the calculation results on the hardware. The comparison of the different filter approaches regarding code size and execution time are done on a 1 GHz ARM Cortex-A8 processor.

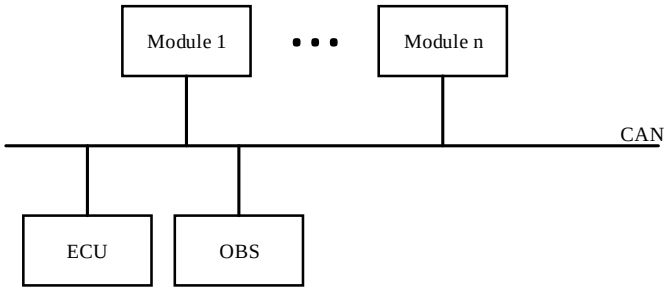

Figure 2: Battery Management System

III. Component Independent Commuter's Cycle Monitoring (CCM)

In order to derive degeneration states of the drivetrain components, a new observer technique is presented. Common methods, which are applied in discrete control theory, such as Luenberger-Observer and Kalman-Filter, have the disadvantage that the underlying discretization techniques require small sample periods. According to Raviv [5], the observers may become instable at low sampling rates due to assumptions during the zero order hold discretization. Schmalstieg [6] states, the process of degeneration exhibits large time constants, as the system components parameters fade irreversibly over several months or even years in a perceivable range. Therefore, control theory methods are enhanced with data storage, where the cycle data (speed and current profile) are also stored as the available measurements.

The idea of this new method is the following: It is assumed that a certain route is taken on a daily or weekly basis, for example, the way to work of a commuter. The cycle information paired with the measurements of the sensor network is stored in a data container (*Figure 3*).

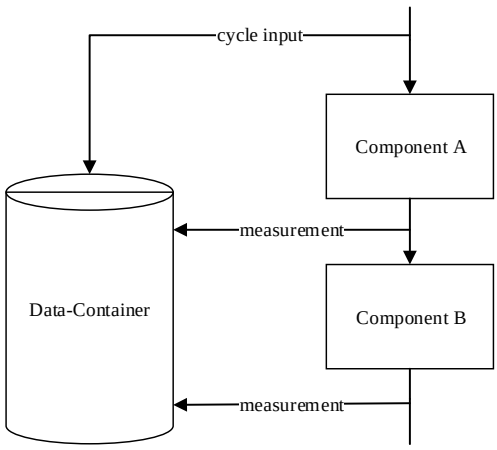

Figure 3: Observer with data container

After a certain period of time, data sets of the commuter cycle can be selected from the data container and compared with one another, if the environmental conditions (e.g. temperature,

traffic situation, driving style) match. This method is named the commuter's cycle monitoring (CCM). Due to the comparison, a trend of degeneration effects is derived that can be used to update the parameters of the state estimators presented in *Chapter IV.B. Figure 4* shows a simulation of the test bed model using parameters that represent a drive train *SOH* from a new car ($SOH_{DT} \approx 100$ %) until approximately 150.000 km ($SOH_{DT} \approx 80$ %). The stimulus signal for all simulation runs was the Artemis Urban cycle. The *SOC* is plotted over the simulated time. It can be noticed, that the *SOC* signature fades in a measurable range over time. Under the assumption that the *SOC* can be estimated, the delta *SOC* is a direct representation of the *SOH* of the drive train. A concept of using the CCM to determine the fading efficiency of the electric motor is given in *Chapter V.B.*

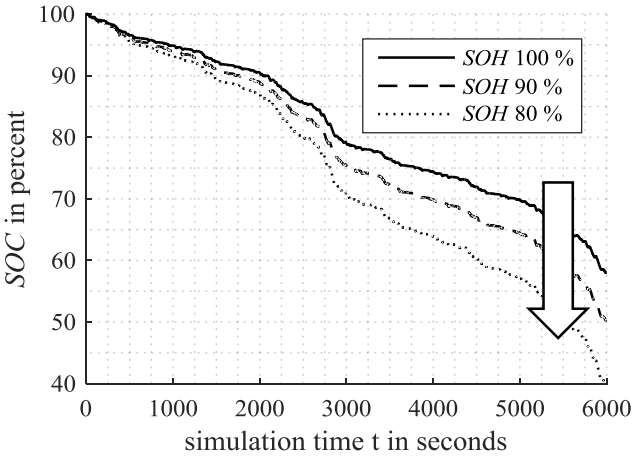

Figure 4: SOC signature for different SOH

In order to implement and test the method, a complex data matching algorithm, accurate GPS data and an actual commuter's route have to be available. Initially, a representative commuter cycle will be used as a test signal on a roller bench. Due to a speed controller implemented on the roller bench control unit, this commuter cycle runs on the roller bench with exactly matching environmental conditions. Using this method, enough data will be produced in order to verify the CCM method, which is the subject of further research. As a second step, the influence of sensor and system noise due to unstable environmental conditions have to be investigated. Also the environmental data that actually have an impact on the measurement have to be defined. However, it is likely that a comparison of multiple data sets will average out this impact.

IV. Traction Battery

The focus of this research is the traction battery. As already investigated by various research institutes in the last decade, estimating the *SOC* of a traction battery by Kalman Filters can be considered as state of the art. The approaches, however, are mostly implemented offline in simulation environments such as MATLAB/Simulink. One of the aims of this research was to implement the most common filter approaches published by the research community and compare them not only regarding the accuracy, but also the code size, the implementation effort and the processing time on an embedded hardware. Since not only the *SOC* should be well known in order to tab the full potential of the battery, the degeneration process also has to be tracked. Plett [7] introduced a joint Kalman Filter in order to estimate the parameters that should correlate with the degeneration. Unfortunately, this correlation cannot be ensured by the presented method since the parameters are used to estimate the states at an optimum. More disadvantages of the joint Kalman Filter are worked out in *Chapter IV.C* and a new method of determining the degeneration process is proposed in *Chapter IV.D.*

A. Modeling battery behavior

Using an electric equivalent circuit is the most common approach to estimate the non-measurable *SOC* of a battery cell. To depict the chemical behavior, it is possible to use a series connection of multiple R-C elements. In this application, the R-C element reproduces the system dynamic. To reproduce the dynamic more accurately, a second R-C element is added as in *Figure 5*. With two R-C elements, the polarization and diffusion effects can be simulated. The model behavior with one and two R-C elements is directly compared. *Equation (1)* is the output equation of the system. According to Jaechan [8] it can be assumed that the matrix multiplication with floating point data types dominates the costs when solving the extended Kalman filter algorithm. Therefore, the computational complexity of the algorithm will be calculated by $\mathcal{O}(n^3)$, which means that the costs will rise cubically with the number of states. This is why an implementation with more than 2 RC-Elements is not seen for embedded solutions.

$$U_{\text{term}} = U_{\text{OCV}} + U_{\text{R}_\text{i}} + U_{\text{RC1}} + \cdots + U_{\text{RC}n} \tag{1}$$

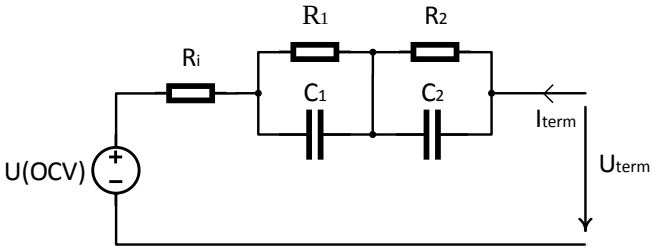

Figure 5: Electric equivalent circuit

There are multiple methods of finding the parameters $(R_\text{i}, R_1, C_1, .., R_n, C_n)$ under laboratory conditions. The method of direct current pulses, which is explained by Varela [9], was used for parameter identification. Independent of the method of measurement, it is possible to determine static parameters that will result in a linear time invariant system (LTI) or one can provide parameters dependent on the SOC, the C-rate and the temperature as a lookup table, hereinafter called a linear parameter variant system (LPV). The open circuit voltage (OCV) curve (including a hysteresis for charge and discharge operation) was measured by current pulses and plotted in *Figure 6.*

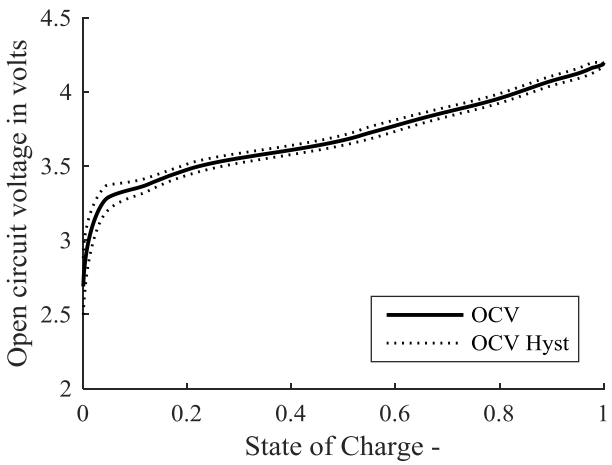

Figure 6: Plot of OCV Curve

It should be noticed that there are no degeneration effects modeled with the parameters, yet. From the equivalent circuit model shown in *Figure 5*, a continuous system description can be deployed using the form of a state space model which is stated in *Equation (2)*:

$$\frac{\partial}{\partial t}\begin{bmatrix} SOC \\ \mathrm{U_{RC1}} \\ \mathrm{U_{RC2}} \end{bmatrix} = \begin{bmatrix} 0 & 0 & 0 \\ 0 & -\frac{1}{C_1 \cdot R_1} & 0 \\ 0 & 0 & -\frac{1}{C_2 \cdot R_2} \end{bmatrix} \cdot \begin{bmatrix} SOC \\ U_{RC1} \\ U_{RC2} \end{bmatrix} + \begin{bmatrix} \frac{1}{C_\mathrm{N}} \\ \frac{1}{C_1} \\ \frac{1}{C_2} \end{bmatrix} \cdot I_{\mathrm{term}}. \tag{2}$$

The state space model shown in *Equation (3)* can be discretized to a time step k with the help of zero order hold. The static parameters were measured by the method of current steps at a *SOC* of 80 % (*Table 1*).

Table 1: Parameter values EKF3LTI

Parameter	*Single cell*	*Cell string (18p)*
C_N	10440 As	187920 As
R_i	25.5 mΩ	1.42 Ω
R_1	16.5 mΩ	0.917 mΩ
C_1	2.3392 F	42.1 F
R_2	23.5 mΩ	1.31 mΩ
C_2	1290.9 F	23236.2 F

$$\boldsymbol{x_{k+1}} = \begin{bmatrix} SOC_{k+1} \\ U_{RC1,k+1} \\ U_{RC1,k+1} \end{bmatrix} = \begin{bmatrix} 1 & 0 & 0 \\ 0 & \exp\left(-\frac{\Delta t_k}{R_1 \cdot C_1}\right) & 0 \\ 0 & 0 & \exp\left(-\frac{\Delta t_k}{R_2 \cdot C_2}\right) \end{bmatrix} \cdot \begin{bmatrix} SOC_k \\ U_{RC1,k} \\ U_{RC2,k} \end{bmatrix} + \begin{bmatrix} \frac{\Delta t_k}{C_\mathrm{N}} \\ \left(1 - exp\left(\frac{-\Delta t_k}{R_1 \cdot C_1}\right)\right) \cdot R_1 \\ \left(1 - exp\left(-\frac{\Delta t_k}{R_2 \cdot C_2}\right)\right) \cdot R_2 \end{bmatrix} \cdot I_{\mathrm{term},k} \tag{3}$$

The system output y_k will be equal to the terminal voltage U_{term} since it is the only measurable value besides the current I_{term} which is already the input vector (or scalar in this case) of the system. It is important to notice that the output equation is dependent on a state (SOC_k). Since $y_k = h(x_k, u_K)$ with respect to the state and the input vector, the output is a nonlinear function. Due to this output nonlinearity, a nonlinear filter approach has to be chosen in order to estimate the *SOC* as well. The output equation can be calculated with Kirchhoff's law to:

$$U_{\mathrm{term},k} = U_{\mathrm{OCV}}(SOC_k) + sign\left(I_{\mathrm{term},k}\right) \cdot U_{\mathrm{hyst}}(SOC_k) + U_{RC1,k} + U_{RC2,k} + R_{i,k} \cdot I_{\mathrm{term},k} \tag{4}$$

The application of a Kalman-Filter for nonlinear problems (extended Kalman-Filer, EKF) is considered as state of the art and is shown by Plett [10]. The seed estimation-error covariance matrix P_0 is developed as

$$P_0 = P_0^T = \begin{bmatrix} e_{SOC}^2 & 0 & 0 \\ sym. & e_{\mathrm{URC1}}^2 & e_{\mathrm{URC1}} \cdot e_{\mathrm{URC2}} \\ sym. & sym. & e_{\mathrm{URC2}}^2 \end{bmatrix} = \begin{bmatrix} 0.25 & 0 & 0 \\ 0 & 0.0625 & 0.0375 \\ 0 & 0.0375 & 0.085 \end{bmatrix}. \tag{5}$$

The process noise of especially the *SOC* is considered low and constant and can therefore be chosen as:

$$Q_{xx} = Q_{xx,k} = \begin{bmatrix} 10^{-9} & 0 & 0 \\ 0 & 0.001 & 0.001 \\ 0 & 0.001 & 0.001 \end{bmatrix}. \tag{6}$$

And a constant measuring noise in the range of the error of the plant model derived from the equivalent circuit

$$R_{yy} = R_{yy,k} = |y_{\mathrm{meas}} - \hat{y}_{3x3}|^2_{\mathrm{max}} = 0.1. \tag{7}$$

The noise and covariance matrices are not used to parametrize the filter algorithm in order to have a physical representation in the system of both the parameters of the equivalent circuit and the noise and covariance matrices.

B. Comparison and discussion of different implementations

In order to compare different Kalman-filter approaches, it was mandatory to set up a toolchain for a fast implementation of the algorithms to an embedded hardware platform. The target for the comparison was the ARM cortex-A8. A real-time framework based on the Linux Debian 7.9 distribution was developed. Within the framework, a hardware abstraction layer (CAN, RTT) and the basic software, which contains the startup functions, the infinite loop and the function, calls to the user functions EKF(1..n) or Spherical Simplex Kalman filter (SPKF). The user functions are developed and tested in MATLAB/Simulink and are then generated to embedded C code as C-functions. After generating the code, the function call in the basic software has to be mapped to the desired algorithm. With the help of this toolchain, it is possible to change the parameters

and the filter approach in Simulink and verify the results in the model. Then the embedded C-code is generated and flashed with the basic software on the target with a round-trip time of under 20 seconds (Simulink model to compiled and flashed solution on the target). *Figure 7* shows the system view of the framework based on the AUTOSAR system description. The measurement modules of the cell voltages have a duty cycle of 25 ms. In order to provide the highest possible accuracy, the provided observer hardware should be able to calculate a Kalman-filter step for every parallel string of the traction battery. In other words, 14 times 8 steps (14 serial cell strings per module, 8 modules per battery) have to be calculated in less than 25 ms.

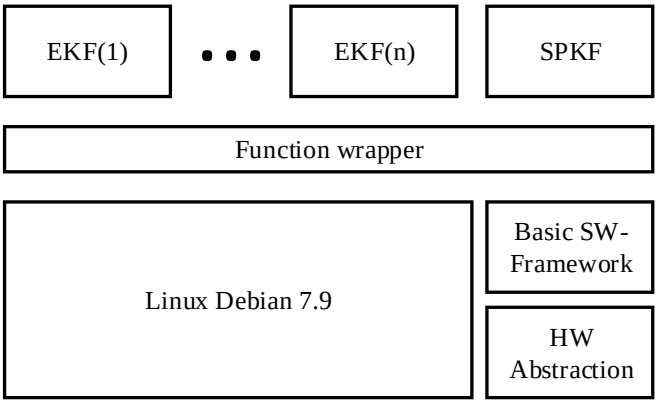

Figure 7: Real-time Framework

As described in *Chapter IV.A* a combination of an EKF with two and three states with both LTI and LPV models are implemented. In addition, a SPKF (Sigma Point Kalman Filter) is implemented with a parameter weighting for the fastest and best convergence, and compared to the EKF methods. The theoretical background of the SPKF can be taken from Julier [11] as it is beyond the frame of this paper. The comparison is done with the fixed parameter set and derived from a step response measurement under a fixed temperature. Various standard driving cycles (NEDC, Artemis Urban and Artemis Rural) and real driving data were taken to test the filters. For the following comparisons, the Artemis Urban cycle was taken. As a dynamic and comparable long cycle, it is well suited for convergence and benchmark comparison. *Figure 8* shows the error over simulation of the EKF using one RC-element with the LPV and LTI system model. It can be seen that the error stays under 2 % in a realistic simulation time of 140 minutes. However it can also be noticed that the error development is neither robust for the LPV nor for the LTI model.

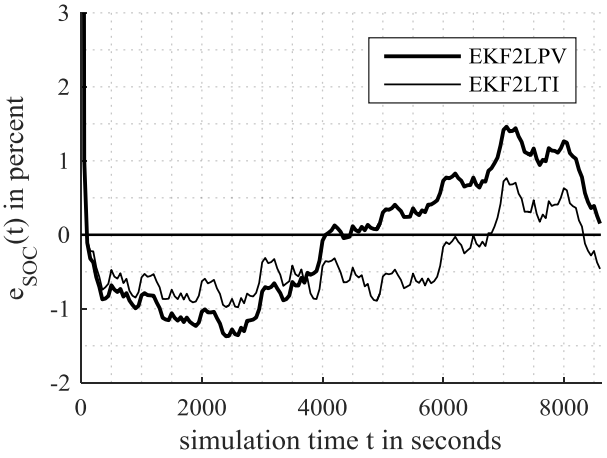

Figure 8: error comparison EKF two states

In a direct comparison to the same filter approach with a three state model (2 R-C elements in the equivalent circuit), much better convergence results can be produced (*Figure 9*). In this case the LPV converges into a tolerance band of 1 % after 8 minutes of simulation. The LTI is in the same range.

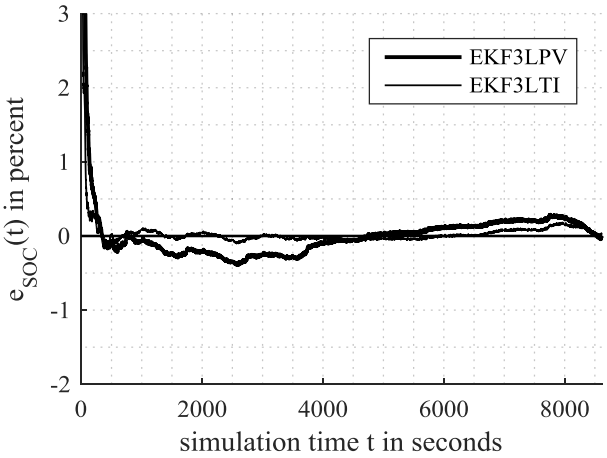

Figure 9: error comparison EKF three states

The SPKF shows promising results (*Figure 10*). Dependent on the driving cycle, the error development of the SPKF was sometimes better and sometimes worse than the EKF3x. With the sigma-points, there are more degrees of freedom for adjusting the filter. In the benchmark, the SPKF was parametrized for fast convergence (SPKF Fast) or for a minimized error (SPKF Best). Compared to the high complexity of the algorithm, however, the results are near to the EKF3x filters. It was shown that the SPKF filter shows different results for different stimulus signals. Because of the high dynamics of the Artemis cycle, the SPKF takes at best almost 30 min for convergence.

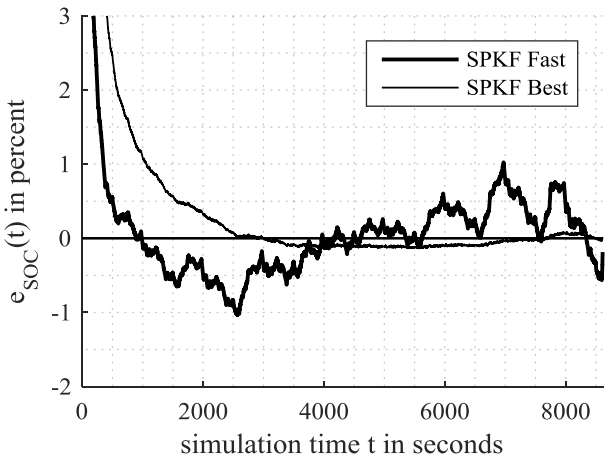

Figure 10: error plot SPKF

After the modeling and parametrization in Simulink, the three filter algorithms are tested on the ARM cortex-A8 with a simulated CAN bus network first (Hardware-in-the-Loop), and on the real environment afterwards. The results in *Table 2* show that the algorithm with parameter sets, implemented as lookup tables, are comparable in execution time and processor load, but they consume almost 12 times as much flash memory. It was not possible to run the Sigma Point Kalman-filter under real time conditions since the ARM Processor would be overloaded (1049 % processor load). A possibility would be to take average values and only calculate one step per module. However, this will lead to significantly larger errors, due to the averaging. The statement of Plett [12] "The computational complexity of SPKF is of the same order as EKF, so the gains are made at little or no additional cost.", could not be met for the used hardware platform.

Table 2: comparison of resource consumption

Filter	t_{mean} ***in µs***	t_{max} ***in µs***	η_{CPU} ***in*** %	***ROM in kB***
EKF2LTI	39.7	6521	44.5	66
EKF2LPV	60.4	4486	67.7	560
EKF3LTI[a]	**57.25**	**6271**	**64.1**	**69**
EKF3LPV	86.2	3811	96.5	800
SPKF	936.6	6848	1049	135

[a.] Best results for convergence and resource need. *(Benchmark on ARM cortex-A8)*

As a conclusion we could imply that the SPKF has the best results regarding convergence, but this is completely out of step regarding the hardware consumption. The EKF with three states and a fixed parameter set was highlighted to have good accuracy and robustness with a low mean processor load. This is why the EKF3LTI will be the underlying filter for further degeneration investigation. If the temperature is the focus of research, it is recommended to use a LPV approach in order to depict the temperature influence in the system behavior.

C. Degeneration parameters of a Lithium Ion Battery

The degeneration of the traction battery is expressed by the following Parameters:

- Actual capacity C_{act}
- Internal resistance R_i

A good overview of the definitions is given by Waag [13]. These parameters are subjected to a degeneration process due to irreversible ageing of the battery (influenced by the DOD, mean *SOC* and the calendric age) and due to the temperature and actual C-rate ($I_{\mathrm{term},k}$). The influence of the C-rate to the nominal capacity expressed by Peukert's equation is neglected in this case because of the low C-rates, which are run on the testbed (1.2 C peak). Additionally, Hausmann [14] determines the Peukert constant *k* to 1.02 for NCA cells. This is very close to an ideal battery, and, thus, the capacity is nearly independent of the current. Detecting the parameters of the traction battery, the use of a Dual Kalman filter is recommended by publications of Walder [15], [16]. In practice, however, this approach has the disadvantage of high computational effort, the risk of instability and, worse, the algorithm does not guarantee the correspondence of the parameters with the true physical values, by name, actual capacity and the inner resistance. This correspondence, however, is mandatory in order to derive an efficiency loss and a value reduction over the lifetime of the energy storage. Due to this fact, an alternative method of detecting the nominal capacity of the traction battery is presented in *Chapter IV.D*. More investigation will be done in the field of estimating the internal resistance of the battery at a system level using vehicle data.

D. Identification of the capacity

An estimation error of the EKF3LTI filter introduced in *Chapter IV.B* is existent due to the fading of R_{i} and C_{act}. The fading of R_i is yet to be neglected since it is the focus of future research on the Smart testbed using CCM. The datasheet of the supplier states a reduction of the nominal capacity of 24 % after 500 standard cycles. A standard cycle is equivalent to a discharge rate of 1 C and a charge rate of 0.7 C at a temperature of 25 °C, respectively. In a real driving cycle, however, the maximum discharge current $I_{term,max}$ and the minimal state of charge SOC_{min} can be considered to be higher. The temperature can also largely differ from the standard cycle. The real degeneration expressed through the C_{act} can, therefore, differ a great amount. By correcting the parameter C_{act} it should be noticed that the degeneration of the capacity after one full cycle has the following magnitude if a linear ageing process is assumed:

$$\frac{\Delta C_{\mathrm{act}}}{C_{\mathrm{act},0}} = \frac{0.24}{500} = 0.048\,\%. \tag{8}$$

A higher degeneration can be due to a lower cell-temperature T_C compared to the previous observed cycle. In order to have a safe operation of the BEV using a maximum load, one has to make sure that the capacity is never estimated too highly:

$$C_{\mathrm{act}} < C_{\mathrm{act,real}}. \tag{9}$$

If the filter estimates a too highly rated *SOC*

$$SOC_{\mathrm{filter}}(t) > SOC_{\mathrm{real}}(t), \qquad \forall t > 0 \tag{10}$$

with a low real *SOC*, a deep discharge cannot be excluded

$$SOC_{\mathrm{filter}}(t') < |SOC_{\mathrm{filter}}(t') - SOC_{\mathrm{real}}(t')|_{\max}. \tag{11}$$

The estimation of the actual capacity is executed in two steps:

(1) feed forward-model

The interconnection between the standard cycle and the actual capacity expressed in *Equation (8)* can be determined by cycle measurements or it can be extracted from the datasheet of the cell manufacturer. Furthermore, a linear relationship between the depth of discharge (*DOD*) of a cycle and the incremental reduction of the nominal capacity caused by the same is presupposed by Schmalstieg [6]. *Equation (7)* is re-dimensioned and factorized with the actual *DOD* solved by the updated nominal capacity

$$C^{-}_{\mathrm{act},k} = C_{\mathrm{act},k-1} - \frac{\delta_{\mathrm{C}}}{n_{\mathrm{cycles}}}(1 - SOC_k), \tag{12}$$

with a reduction of the nominal capacity

$$\delta_{\mathrm{C}} = C_{\mathrm{act},0} - C_{\mathrm{act}}(n_{\mathrm{cycles}}). \tag{13}$$

(2) feedback-correction

The correction of the provisionally nominal capacity $C^{-}_{act,k}$ is used to minimize the primary error

$$e_1 = C^{-}_{\mathrm{act},k} - C_{\mathrm{act,real}}. \tag{14}$$

The primary error induces a secondary error of the state of charge (*SOC*) estimation

$$e_2 = SOC_{\mathrm{est}} - SOC_{\mathrm{real}} \sim f(e_1, \int I_{\mathrm{term}}) \tag{15}$$

of the EKF3LTI. The nominal capacity, however, can only be measured with the sought accuracy under laboratory conditions because a cell has to be completely charged and discharged with the possibility of an accurate current measuring unit. The secondary error e_2 can be approximately estimated for a parked, not fully charged BEV by utilizing the inverse OCV. As seen in *Table 1*, the time constant of the impedance R-C element, a maximum time constant $\tau_{2,max} = 30$ s, a capacitance resistance of $R_{2,\max} = 1.31\ \mathrm{m\Omega}$ and a maximum discharge current of $I_{\mathrm{term,max}} = 180$ A is presumed. After 300 seconds, the maximum possible voltage drop is

$$\begin{aligned} \mathrm{U_{RC2}}(t = 300\mathrm{s}) &= R_{2,\max} \cdot I_{\mathrm{term,max}} \cdot \exp\left(-\frac{300\mathrm{s}}{\tau_{2,\max}}\right) \\ &= -0.0107\ \mathrm{mV}. \end{aligned} \tag{16}$$

Further relaxation processes cannot be observed. For a given state of charge, the terminal voltage calculates to

$$\begin{aligned} \xi(SOC_{\mathrm{real}}) &\coloneqq U_{OCV}(SOC_{\mathrm{real}}) - U_{Hyst}(SOC_{\mathrm{real}}) \\ &\approx U_{\mathrm{kl}}(t = 300s). \end{aligned} \tag{17}$$

Since the terminal voltage can be assumed to be constant in this case, the made approximation is sufficiently accurate. The difference function ξ of the OCV-function deducting the voltage hysteresis is a continuous, strictly monotonic mapping. Hence, the inverse ξ^{-1} does exist. The higher the error of the current capacity estimation $C^{-}_{\mathrm{act},k}$ and the higher the nominal depth of discharge, the higher the estimation error e_2:

$$\begin{aligned} \Delta SOC &= SOC_{\mathrm{est}} - SOC_{\mathrm{real}} \\ &\cong \frac{C^{-}_{\mathrm{act,k}} - C_{\mathrm{act,real}}}{C_{\mathrm{act,real}}} \cdot (1 - SOC_{\mathrm{real}}). \end{aligned} \tag{18}$$

$C_{\mathrm{act},real}$ is substituted with the corrected estimation $C_{\mathrm{act},k}$ and the equation (18) solved to $C_{\mathrm{act},k}$ results in

$$C_{\mathrm{act},k} = \omega_{\mathrm{d}} \cdot \frac{C^{-}_{\mathrm{act},k}}{\frac{SOC_{\mathrm{est}} - SOC_{\mathrm{real}}}{1 - SOC_{\mathrm{real}}} + 1} \tag{19}$$

using a damping factor $\omega_d \leq 1$ for preventing instability.

In The CCM is not yet applied to the alternative of estimating the capacity without using an ideal state estimator (Kalman-Filter), presented here. Future work will show whether applying CCM will result in better estimations or whether, more likely, a combination of this method and CCM is advised.

E. Methods of verification

The traction battery construction, which uses a clamping method for contacting the battery cells, offers the possibility of disassembling the battery modules in order to measure the parameters R_{i} and C_{act} on a cell level under laboratory conditions. This parameter verification will be done every 5,000 km of driven distance of the test bed. Since not all 2016 cells can be measured, only 10 cells of each module are chosen to deliver the benchmark. After the measurement, the battery modules can be assembled in the same manner as before. This method offers reliable results to verify the estimation approach over the lifetime of a battery pack.

In addition to the cell test, it is possible to run a driving cycle on a roller test bench environment using a speed control mechanism. The battery data can be saved and compared to datasets that were produced under the exact same conditions (e.g. speed profile, start *SOC*, ambient temperature). The comparison of the data sets reflect a trend of the degeneration.

V. Degeneration of the Power Unit

The power unit, consisting of the DC-AC converter and the electric machine is hooked up with an observer unit, based on a second ARM Cortex A8 rapid control prototype hardware. The real time framework introduced in *Chapter IV.B* is reused for this solution. The DC and AC power is measured by two automotive voltage-current sensor units (Isabellenhuette IVT-MOD, 0.1% accuracy). The motor speed is measured by the motor control function. With an additional sensor, the motor torque is measured. *Figure 11* shows an overview of the electric drive train, which is installed in the test bed. In the field of automotive technology, it will be likely that the components are designed less robustly or an overloading of the components will be tolerated in order to save weight and costs.

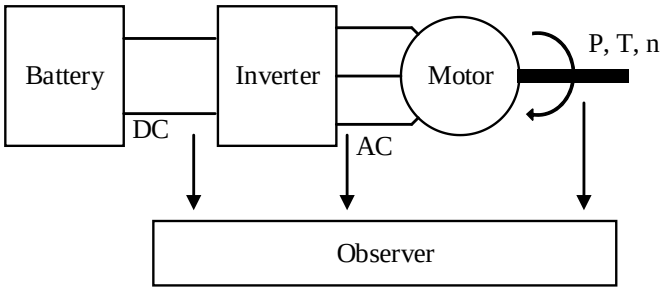

Figure 11: Electrical Power Unit

A. *Efficiency fading of DC-AC Converters*

The DC-AC converter (inverter) adapts the DC current provided by the traction battery to a three phases AC current pulled by the electric induction motor. In order to identify the losses of the inverter, a component view of the semiconductors (Power Mosfets) is proposed.

It is important to notice that both, the conduction losses and the switching losses are independent of time or switching numbers for common automotive Mosfets. Therefore, an ageing process cannot be noted, if the semiconductor runs under normal temperature conditions (Datasheet Mosfets: -55 to 175°C), which was investigated by Saha [17]. Because of the active cooling circuit and a temperature monitoring, normal conditions can be guaranteed. Furthermore, the electrical DC-power and AC-power is measured by the sensor network. Even though it is unlikely to drop, the efficiency can be tracked during operation, and an efficiency fading will be noticed by the system. A CCM implementation is renounced due to high data management effort with low profit in system information.

B. *Lifetime monitoring of induction motor*

Since a method like CCM only detects an efficiency loss in the entire drivetrain, an accurate knowledge of the electric motor is required. The possible degeneration effects of an induction motor are given by Ojo [18]. The degeneration effects are evaluated with respect to a possible efficiency fading over a lifetime. According to Rothe [19] induction motor degeneration can be grouped into four classes: mechanical, electrical, environmental and thermal effects. However, most of the ageing effects will lead to fatal failure of the IM.

Erbay [20] makes detailed analyses of common failures of modern induction motors with the background of stationary machines. It is supposed that the same behavior can be adapted to a mobile application of induction motors. A detailed summary of the failure-modes of the stator can be found in the dissertation of Mayer [21]. Basically there are three parts that are influenced by degeneration effects (*Figure 12*):

- Stator, including the isolated windings
- Rotor
- Bearing of shaft to rotor.

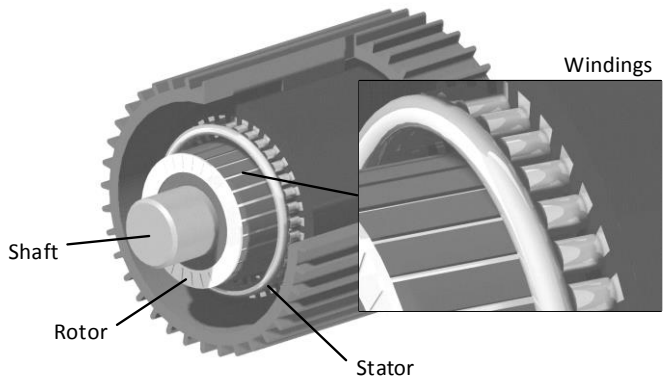

Figure 12: Induction Motor

According to Erbay, an analysis of the power or current signature and the temperature applied with a data-fusion will provide accurate knowledge about the actual health of the motor. Furthermore, an apriority estimation about the end of life (EOL) is made by Huger [22], which is confined, however, in this paper in order to compliment the CCM approach. A total failure of the motor will be detected by the electronic control unit and the information will be passed to the user. In focus is the degeneration of the induction motor during a lifetime, which results in efficiency or power fading.

First of all, the motor's behavior can deviate from the predicted behavior, due to manufacturing tolerances. One effect that can lead to power fading over a lifetime is a short circuiting of the windings. Having a short circuit between two phases will lead into failure of the IM if a special machine design is not chosen that allows control even under special failure conditions. A short circuit in between one phase will result in a lower windings number of one phase or a partial discharge, which will lead to an irregularly running of the machine. Also, the control mechanism is likely to be less efficient. The one phase short can be emulated in a trivial manner. The effect will be measured and saved into an updated motor efficiency diagram. Having the updated diagram, a method of using the current and temperature profile will be derived.

VI. Conclusion

The focus of this paper's research was the drive train components: traction battery, inverter and induction motor of common BEVs. The aim was not to investigate the cause or to predict, but to detect degeneration processes inside these components. State estimators for batteries are considered state of the art. However, a benchmark of the most promising filter approaches was done in order to suggest a suitable solution. The state estimator was enhanced with parameter detection based on the introduced CCM. This method will show a trend of the overall degeneration of the drivetrain, whereat the battery degeneration is uncertain and the inverter efficiency over a lifetime is regarded as static. The motor degeneration will be detected by an enhanced observer model, which will be the subject of further research, using the same test bed. Using a long term data procedure, robust information about the *SOH* of the battery and the function level of the drive train can be given. Using the electrified Smart testbed, enhanced with parametrized simulation model results of using CCM in order to calculate value and the efficiency of the drivetrain over a lifetime, will be in focus of further research.

Acknowledgment

The research which is described in this paper was founded by the BFS – Bavarian Research Foundation through the collaborative project FORELMO between 2013 and 2015. Special thanks go to C. Reiter and C. Hildenbrand by supporting this research in a great manner.

Contributions

J.A. initiated the work on CCM with the objective to implement the method on the electrified Smart using a real-time environment. The testbed – electrified Smart was engineered by P.W. and J.A. in 2015. L.H. supported the research with his

scientific background of induction motors. M.B. complemented the research with his knowledge in modelling and ageing mechanisms of lithium ion batteries. M.L. made an essential contribution to the conception of the research project and revised the paper critically for important intellectual content. M.L. gave final approval of the version to be published and agrees to all aspects of the work. As a guarantor, M.L. accepts responsibility for the overall integrity of the paper.

REFERENCES

[1] ADAC, "Gebrauchtwagenpreise 2015," *adac.de*, 2015. [Online]. Available: https://www.adac.de/_mmm/pdf/gebrauchtwagenpreise_53800.pdf.

[2] M. Baumann, S. Rohr, and M. Lienkamp, "Development and Investigation of a modular stationary Second Life Storage System," in *Conference on Future Automotive Technology*, 2016.

[3] Melissa Bowler and M. Bowler, "Battery Second Use : A Framework for Evaluating the Combination of Two Value Chains," *All Diss.*, no. May, pp. 1–32, 2014.

[4] J. Neubauer and A. Pesaran, "The ability of battery second use strategies to impact plug-in electric vehicle prices and serve utility energy storage applications," *J. Power Sources*, vol. 196, no. 23, pp. 10351–10358, 2011.

[5] D. Raviv and E. W. Djaja, "Daniel Raviv and Eddy W. Djaja," *IEEE Control Syst.*, vol. 0272–1708/, pp. 52–57, 1999.

[6] J. Schmalstieg, S. Käbitz, M. Ecker, and D. U. Sauer, "A holistic aging model for Li(NiMnCo)O2 based 18650 lithium-ion batteries," *J. Power Sources*, vol. 257, no. February 2016, pp. 325–334, 2014.

[7] G. L. Plett, "Dual and Joint EKF for Simultaneous SOC and SOH Estimation," *Proc. 21st Electr. Veh. Symp.*, pp. 1–12, 2005.

[8] J. Lim, T. Kim, and D. Hong, "Estimating the number of competing terminals without a state variation detector in wireless LAN," *EURASIP J. Adv. Signal Process.*, vol. 2013, no. 1, p. 182, 2013.

[9] J. Varela, D. Castro, M. Jozef, J. Andreasen, R. Esteves, J. V Barreras, C. Pinto, R. De Castro, E. Schaltz, M. Swierczynski, S. J. Andreasen, and R. E. Ara, "An Improved Parametrization Method for Li-ion Linear Static Equivalent Circuit Battery Models Based on Direct Current Resistance Measurement," in *Proceedings of the International Conference on Sustainable Mobility*, 2015, pp. 1–8.

[10] G. L. Plett, "Extended Kalman filtering for battery management systems of LiPB-based HEV battery packs - Part 3. State and parameter estimation," *J. Power Sources*, vol. 134, no. 2, pp. 277–292, 2004.

[11] S. Julier, J. Uhlmann, and H. F. Durrant-Whyte, "A New Method for the Nonlinear Transformation of Means and Covariances in Filters and Estimators," *IEEE Trans. Automat. Contr.*, vol. 51, no. 12, pp. 1938–1943, 2006.

[12] G. L. Plett, "Sigma-point Kalman filtering for battery management systems of LiPB-based HEV battery packs. Part 1: Introduction and state estimation," *J. Power Sources*, vol. 161, no. 2, pp. 1356–1368, 2006.

[13] W. Waag, C. Fleischer, and D. U. Sauer, "Critical review of the methods for monitoring of lithium-ion batteries in electric and hybrid vehicles," *J. Power Sources*, vol. 258, pp. 321–339, 2014.

[14] A. Hausmann and C. Depcik, "Expanding the Peukert equation for battery capacity modeling through inclusion of a temperature dependency," *J. Power Sources*, vol. 235, no. February 2016, pp. 148–158, 2013.

[15] G. Walder, C. Campestrini, S. Kohlmeier, M. Lienkamp, and A. Jossen, "Functionality and Behaviour of Different Kalman Filters Related to a Modular Conference on Future Automotive Technology : Focus Electromobility," in *Conference on Future Automotive Technology*, 2013, pp. 1–8.

[16] G. Walder, C. Campestrini, M. Lienkamp, and A. Jossen, "Adaptive State and Parameter Estimation of Lithium-Ion Batteries Based on a Dual Linear Kalman Filter -," pp. 1–10.

[17] S. Saha, J. R. Celaya, V. Vashchenko, S. Mahiuddin, and K. F. Goebel, "Accelerated aging with electrical overstress and prognostics for power MOSFETs," *Energytech 2011*, pp. 1–6, 2011.

[18] O. Ojo, O. Osaloni, and P. Kshirsagar, "Type Machine Drives Under Various Fault Conditions .," *Ind. Appl. Conf. IEEE*, pp. 1533–1540, 2002.

[19] R. Rothe and K. Hameyer, "Life expectancy calculation for electric vehicle traction motors regarding dynamic temperature and driving cycles," *2011 IEEE Int. Electr. Mach. Drives Conf. IEMDC 2011*, pp. 1306–1309, 2011.

[20] A. S. Erbay, "Multi-Sensor Fusion for Induction Motor Aging Analysis and Fault Diagnosis," 1999, pp. 35–41.

[21] J. S. Mayer, "Analyse und Behandlung von unsymmetrischen Zuständen in fehlertoleranten PM-Synchronmaschinen," in *PhD Proposal*, 2015, vol. 1, pp. 157–176.

[22] D. Huger and D. Gerling, "An advanced lifetime prediction method for permanent magnet synchronous machines," *2014 Int. Conf. Electr. Mach.*, pp. 686–691, 2014.